24th COBEM - 2017

24th ABCM International Congress of Mechanical Engineering
December 3-8, 2017, Curitiba, PR, Brazil

COBEM-2017-2372
THEORETICAL AND EXPERIMENTAL ANALYSIS OF HYDRODYNAMIC AND THERMOHYDRODYNAMIC MODELS OF CYLINDRICAL BEARINGS

Jefferson Silva Barbosa
Leonardo Campanine Sicchieri
Arinan Dourado Guerra Silva
Aldemir Ap Cavalini Jr
Valder Steffen Jr
LMEst - Structural Mechanics Laboratory, Federal University of Uberlandia, School of Mechanical Engineering, Av. João Naves de Ávila, 2121, Uberlândia, MG, 38408-196, Brazil.
e-mail: jsbarbosa@ufu.br
e-mail: leo_sicchieri@ufu.br
e-mail: arinandourado@ufu.br
e-mail: aacjunior@ufu.br
e-mail: vsteffen@ufu.br

Abstract. *The hydrodynamic bearings represent an important component of rotating machines due to their large use in the industry. In this case, the load is supported by a thin film of lubricant that separates the shaft from the bearing (i.e., there is no direct contact between metal parts). Thus, this subsystem can theoretically offer infinite life, considering that the rotor operates under safe dynamic conditions and with clean lubricant. Different mathematical models can be used to represent the dynamic behavior of hydrodynamic bearings. This work is dedicated to the comparation between the results obtained by using the hydrodynamic (HD) and thermohydrodynamic (THD) models for cylindrical bearings. The HD model is based on the solution of the classical Reynolds equation, in which the oil viscosity is considered constant along the film, disregarding thermal effects. In the THD model, the Reynolds equation is modified to take into account the viscosity variation due to temperature gradients generated in the bearing. The results obtained by using both models are compared in terms of the maximum pressure, minimum oil film thickness, and the equilibrium position of shaft for a given applied load.*

Keywords: *cylindrical hydrodynamic bearings, hydrodynamic model, thermohydrodynamic model.*

1. INTRODUCTION

According to Meggiolaro (1996), the computational simulation of rotating machines is an indispensable resource for engineers. It allows a comprehensive understanding about the dynamic behavior of the system, considering the number of variables involved on the problem. Thereby, a mathematical model capable of representing satisfactorily the dynamic behavior of a rotating machine is obtained by taking into account various subsystems. The bearings are one of the most critical subsystems of the rotor system, influencing significantly on the performance, life, and reliability of the machine. According to Vance et al. (2010), many problems in rotating systems can be attributed to the design and application of the bearings. Thus, understanding the physical phenomena that involve the bearings is essential to improve the dynamic performance of the system (Cavalini Jr et al., 2014).

The hydrodynamic bearings represent an important component of rotating machines due to their large use in the industry (Riul, 1988). In this case, the load is supported by a thin film of lubricant that separates the shaft from the bearing (i.e., there is no direct contact between metal parts). Thus, this subsystem can theoretically offer infinite life, considering that the rotor operates under safe dynamic conditions and with clean lubricant (Vance et al., 2010). It is worth mentioning that due to the oil film, the damping effect on hydrodynamic bearings is more pronounced than in rolling bearings, which is beneficial in machines that go through critical speeds during startup and stop down procedures. Due to the high load capacity, hydrodynamic bearings are commonly used in large rotating machines, such as hydroelectric plant generating units.

Cylindrical hydrodynamic bearings present consolidated mathematical models (Childs, 1993). Such models are able to determine the pressure field on the oil film and, consequently, the hydrodynamic supporting forces. In the HD model of cylindrical bearings, the thermal effects are neglected. Thus, the oil film viscosity is constant throughout the oil film (Riul, 1988). The thermal effects are considered only in THD model. In this case, the Reynolds equation is initially solved for a uniform oil film temperature to determine the supporting pressure distribution and the fluid velocity field. The temperature of the oil film along the bearing is obtained from the solution of the energy equation, which depends on the fluid velocity field. Consequently, the pressure distribution can be determined considering the resulting oil film temperature. This process continues until convergence is achieved. In the equilibrium condition, the hydrodynamic supporting forces and the external load applied to the shaft are equal.

In this condition, the results obtained by using the HD and THD models for cylindrical bearings are compared. The HD model is based on the solution of the classical Reynolds equation, in which the oil viscosity is considered constant along the film, disregarding thermal effects. In the THD model, the Reynolds equation is modified to take into account the viscosity variation due to temperature gradients generated in the bearing. For a given external load, the results obtained by using both models are compared in terms of the maximum pressure, minimum oil film thickness, and the equilibrium position of shaft. The maximum temperature obtained by using the THD model is also presented. The results were obtained by considering a cylindrical bearing installed on the Francis hydro power unit.

2. CYLINDRICAL BEARINGS

In this work, the hydrodynamic forces are determined from Reynolds equation modified in its dimensionless form (Eq. (1)). In this approach, the energy equation is inserted into mathematical modeling considering that the temperature is constant in axial direction of the bearing and neglecting the conduction between the lubricating fluid and the surrounding parts (shaft and bearing) according to the modeling proposed by Daniel (2012). It is noted that there is no variation of pressure in the radial direction due to the thin oil film thickness. Figure 1 represents a hydrodynamic cylindrical bearing and its main geometrical parameters.

$$\left(\frac{1}{2\pi}\right)^2 \frac{\partial}{\partial \bar{x}}\left(\bar{F}_2 \bar{h}_h^{\,3} \frac{\partial \bar{p}_h}{\partial \bar{x}}\right)+\left(\frac{R}{L_h}\right)^2 \frac{\partial}{\partial \bar{z}}\left(\bar{F}_2 \bar{h}_h^{\,3} \frac{\partial \bar{p}_h}{\partial \bar{z}}\right)=\left(\frac{1}{2\pi}\right)\frac{\partial}{\partial \bar{x}}\left[\bar{h}_h\left(1-\frac{\bar{F}_1}{\bar{F}_0}\right)\right]+\frac{\partial \bar{h}_h}{\partial \bar{t}} \tag{1}$$

in which,

$$\begin{aligned}
\bar{F}_0 &= \int_0^1 \frac{1}{\bar{\mu}} d\bar{y} \\
\bar{F}_1 &= \int_0^1 \frac{\bar{y}}{\bar{\mu}} d\bar{y} \\
\bar{F}_2 &= \int_0^1 \frac{\bar{y}}{\bar{\mu}}\left(\bar{y}-\frac{\bar{F}_1}{\bar{F}_0}\right) d\bar{y}
\end{aligned} \tag{2}$$

being $\bar{x} = x/2\pi R$ e $\bar{z} = z/L_h$ the dimensionless coordinates into X and Z directions, respectively, R is the shaft radius, L_h is the length of bearing, C is the radial clearance of bearing, e is the eccentricity (radial displacement from

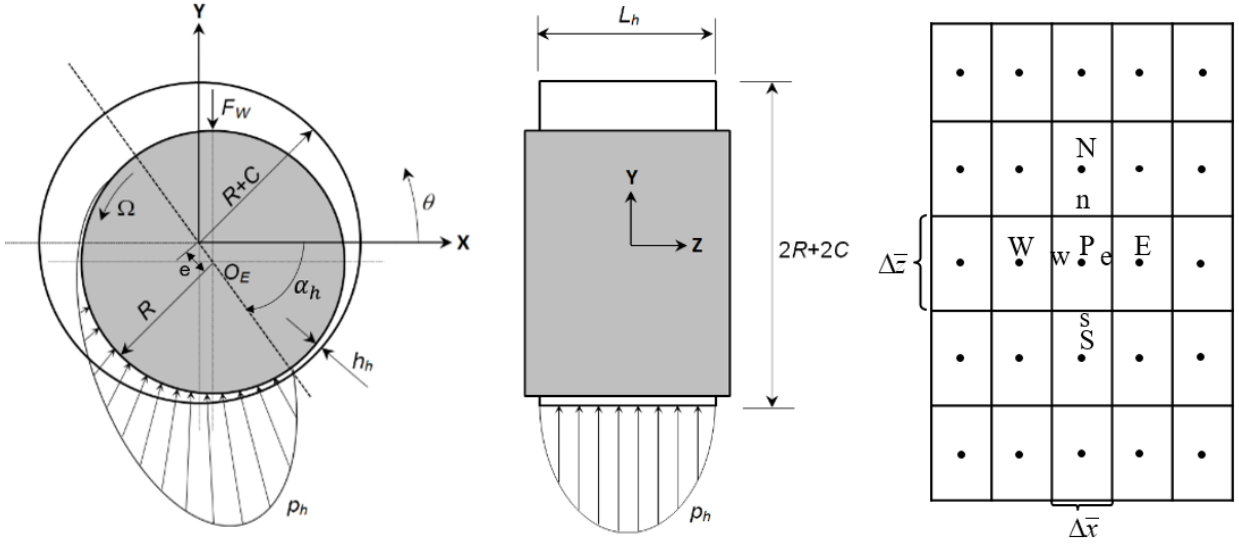

a) XY plane b) YZ plane c) Discretized mesh.

Figure 1. Physical modeling of hydrodynamic cylindrical bearing.

the center of shaft O_E to the center of bearing), α_h is the angle that defines the equilibrium, ω the rotation speed of shaft, $\bar{\mu} = \mu/\mu_0$ it is the dimensionless oil viscosity (μ_0 is reference viscosity), $\bar{p}_h = p_h(x,z)/(\mu_0 \omega R/C)$ is the bearing hydrodynamic pressure (dimensionless), $\bar{t} = \omega t$ is the temporal dimensionless coordinate and $\bar{h}_h = 1 - \bar{x}_R \cos\theta - \bar{y}_R \sin\theta$ it is the dimensionless oil film thickness, in which, $\bar{x}_R$ and $\bar{y}_R$ are dimensionless coordinate of the center of shaft, obtained from $\bar{x}_R = E\cos\alpha_h$ and $\bar{y}_R = E\sin\alpha_h$, where $E = e/C$.

Applying the finite volume method in Eq. (1), the following equation is obtained:

$$C_P \bar{P}_P + C_E \bar{P}_E + C_W \bar{P}_W + C_N \bar{P}_N + C_S \bar{P}_S = B_P \tag{3}$$

with

$$\begin{aligned}
C_E &= \left(\frac{1}{2\pi}\right)^2 \frac{\Delta\bar{z}}{\Delta\bar{x}} \bar{F}_{2e} \bar{h}_{he}^3 \\
C_W &= \left(\frac{1}{2\pi}\right)^2 \frac{\Delta\bar{z}}{\Delta\bar{x}} \bar{F}_{2w} \bar{h}_{hw}^3 \\
C_N &= \left(\frac{R}{L_h}\right)^2 \frac{\Delta\bar{x}}{\Delta\bar{z}} \bar{F}_{2n} \bar{h}_{hn}^3 \\
C_S &= \left(\frac{R}{L_h}\right)^2 \frac{\Delta\bar{x}}{\Delta\bar{z}} \bar{F}_{2s} \bar{h}_{hs}^3 \\
C_P &= -\left(C_E + C_W + C_N + C_S\right) \\
B_P &= \left(\frac{1}{2\pi}\right)\left[\bar{h}_{he}\left(1 - \frac{\bar{F}_{1e}}{\bar{F}_{0e}}\right) - \bar{h}_{hw}\left(1 - \frac{\bar{F}_{1w}}{\bar{F}_{0w}}\right)\right]\Delta\bar{z} + \frac{\partial \bar{h}_{hp}}{\partial \bar{t}}\Delta\bar{x}\Delta\bar{z}
\end{aligned} \tag{4}$$

To obtain the pressure field, Eq. (3) is evaluated for each of the considered finite volumes. Then, this set of equations can be written in the form of a linear system, where $\{P\}$ represents the vector containing the pressures of all control volumes, $[C]$ is the matrix of the coefficients obtained from Eq. (4), and $\{B\}$ represents the source terms of each finite volumes. The solution of the linear system can be obtained directly through the inversion of the matrix $[C]$ (Eq. (5)), considering the boundary conditions showed in Eq. (6).

$$\{P\} = [C]^{-1}\{B\} \tag{5}$$

$$\begin{cases} \bar{p}_h(\bar{x},\bar{z}) < 0 \rightarrow \bar{p}_h(\bar{x},\bar{z}) = 0 \\ \bar{p}_h(\bar{x},0) = \bar{p}_h(\bar{x},1) = 0 \end{cases} \tag{6}$$

The temperature distribution in the oil film can be determined by means of the energy equation in its two-dimensional form applied to an incompressible fluid (Eq. (7)), since the heat transfer in the bearing occurs predominantly in the radial direction, disregarding the energy transfer in the axial direction (Daniel, 2012).

$$\rho c_p \left(u\frac{\partial T}{\partial x} + v\frac{\partial T}{\partial y} \right) = k\left(\frac{\partial^2 T}{\partial x^2} + \frac{\partial^2 T}{\partial y^2} \right) + \mu \cdot \Phi$$

$$\Phi = 2\cdot\left[\left(\frac{\partial u}{\partial y}\right)^2 + \left(\frac{\partial w}{\partial y}\right)^2 \right] + \left(\frac{\partial u}{\partial y} + \frac{\partial v}{\partial x}\right)^2 + \left(\frac{\partial w}{\partial y}\right)^2 + \left(\frac{\partial w}{\partial x}\right)^2 \tag{7}$$

where c_p and k are specific heat capacity and thermal conductivity of fluid, respectively, and u, v, and w are the velocity components of the fluid along the X, Y, and Z directions, respectively, as shows the Eq. (8).

$$\begin{aligned} u &= \frac{\partial p_h}{\partial x}\cdot\int_0^{h_h}\frac{y}{\mu}dy + \left(\frac{\omega R}{F_0} - \frac{F_1}{F_0}\frac{\partial p_h}{\partial x}\right)\cdot\int_0^{h_h}\frac{dy}{\mu} \\ w &= \frac{\partial p_h}{\partial z}\cdot\int_0^{h_h}\frac{y}{\mu}dy + \left(\frac{\partial p_h}{\partial z}\cdot\frac{F_1}{F_0}\right)\cdot\int_0^{h_h}\frac{dy}{\mu} \\ v &= -\int_0^{h_h}\left(\frac{\partial u}{\partial x} + \frac{\partial w}{\partial z}\right)dy + \frac{\partial h_h}{\partial t} \end{aligned} \tag{8}$$

Similar to the solution adopted to the Reynolds equation, the Energy equation must be solved by using numerical methods. According to Daniel (2010), due to oil film thickness variation along the circumferential direction, a coordinate transformation is used to change the non-uniform physical mesh into a uniform computational mesh, which will be discretized by using the finite volume method. Thus, the coordinates x and y are replaced by the dimensionless coordinates $\xi = x/2\pi R$ and $\eta = y/h_h$. Figure 2 shown the mesh resulting from the applied coordinate transformation.

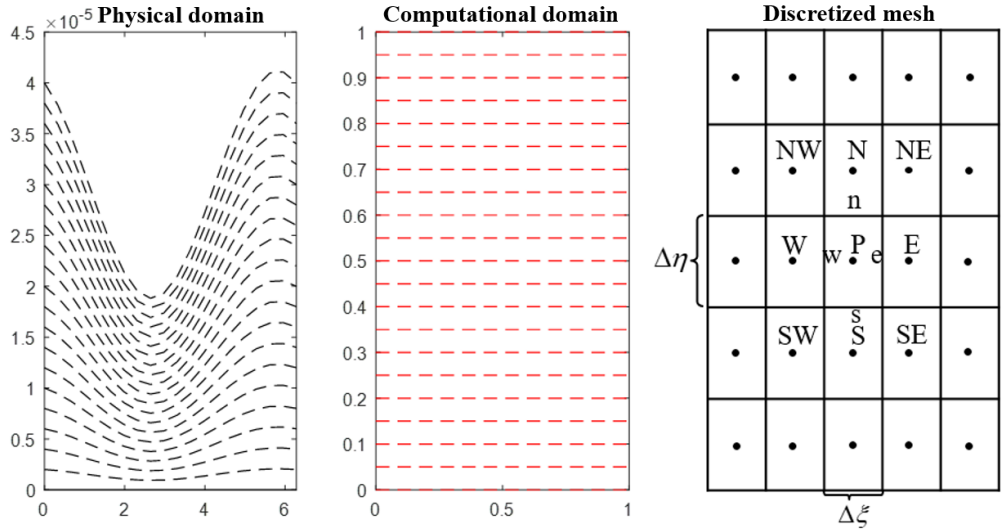

Figure 2. Construction of the computational mesh.

Applying the finite volume methods in Eq. (7), the following equation is obtained:

$$A_P T_P + A_E T_E + A_W T_W + A_N T_N + A_S T_S + A_{NE} T_{NE} + A_{NW} T_{NW} + A_{SE} T_{SE} + A_{SW} T_{SW} = B_P \tag{8}$$

where,

$$
\begin{aligned}
A_E &= \dot{M}_e\left(\frac{1}{2}-\bar{\alpha}_e\right)-\frac{D_{11}}{\Delta\xi}\bar{\beta}_e-\left(\frac{D_{21n}-D_{21s}}{4\Delta\xi}\right)\\
A_W &= -\dot{M}_w\left(\frac{1}{2}+\bar{\alpha}_w\right)-\frac{D_{11w}}{\Delta\xi}\bar{\beta}_w+\frac{D_{21n}-D_{21s}}{4\Delta\xi}\\
A_N &= \dot{M}_n\left(\frac{1}{2}-\bar{\alpha}_n\right)-\frac{D_{22n}}{\Delta\eta}\bar{\beta}_n-\left(\frac{D_{12e}-D_{12w}}{4\Delta\eta}\right)\\
A_S &= -\dot{M}_s\left(\frac{1}{2}+\bar{\alpha}_s\right)-\frac{D_{22s}}{\Delta\eta}\bar{\beta}_s-\left(\frac{D_{12w}-D_{12e}}{4\Delta\eta}\right)\\
A_{NE} &= -\frac{D_{12e}}{4\Delta\eta}-\frac{D_{21n}}{4\Delta\xi} \qquad A_{SE} = \frac{D_{12e}}{4\Delta\eta}+\frac{D_{21s}}{4\Delta\xi}\\
A_{NW} &= \frac{D_{12w}}{4\Delta\eta}+\frac{D_{21n}}{4\Delta\xi} \qquad A_{SW} = -\frac{D_{12w}}{4\Delta\eta}-\frac{D_{21s}}{4\Delta\xi}\\
A_P &= -\left(A_E+A_W+A_N+A_S+A_{NE}+A_{SE}+A_{NW}+A_{SW}\right)
\end{aligned}
\tag{9}
$$

being $\bar{\alpha}$ and $\bar{\beta}$ interpolation coefficients determined by using the Peclet number (Maliska, 2004) and

$$
\begin{aligned}
\dot{M}_e &= \left(\rho h_{he} u_e\right)\Delta\eta & \dot{M}_w &= \left(\rho h_{hw} u_w\right)\Delta\eta\\
\dot{M}_n &= \rho\left(2\pi R v_n-\eta_n\left.\frac{\partial h_h}{\partial\xi}\right|_n u_n\right)\Delta\xi & \dot{M}_s &= \rho\left(2\pi R v_s-\eta_s\left.\frac{\partial h}{\partial\xi}\right|_s u_s\right)\Delta\xi\\
D_{11e} &= \frac{k}{c_p}\left(\frac{1}{2\pi R h_{he}}\right)h_{he}^2\Delta\eta & D_{11w} &= \frac{k}{c_p}\left(\frac{1}{2\pi R h_{hw}}\right)h_{hw}^2\Delta\eta\\
D_{12e} &= -\frac{k}{c_p}\left(\frac{1}{2\pi R h_{he}}\right)\left[\eta_e h_{he}\left(\frac{\partial h_h}{\partial\xi}\right)\Big|_e\right]\Delta\eta & D_{12w} &= -\frac{k}{c_p}\left(\frac{1}{2\pi R h_{hw}}\right)\left[\eta_w h_{hw}\left(\frac{\partial h_h}{\partial\xi}\right)\Big|_w\right]\Delta\eta\\
D_{21n} &= -\frac{k}{c_p}\left(\frac{1}{2\pi R h_{hn}}\right)\left[\eta_n h_{hn}\left(\frac{\partial h_h}{\partial\xi}\right)\Big|_n\right]\Delta\xi & D_{21s} &= -\frac{k}{c_p}\left(\frac{1}{2\pi R h_{hs}}\right)\left[\eta_s h_{hs}\left(\frac{\partial h_h}{\partial\xi}\right)\Big|_s\right]\Delta\xi\\
D_{22n} &= \frac{k}{c_p}\left(\frac{1}{2\pi R h_{hn}}\right)\left[\left(2\pi R\right)^2+\left(\eta_n\left(\frac{\partial h_h}{\partial\xi}\right)\Big|_n\right)^2\right]\Delta\xi & B_P &= \left(\frac{1}{2\pi R h_{hp}}\right)\left(\omega R\right)^2\frac{\mu}{c_p}\bar{\Phi}_P\Delta A
\end{aligned}
\tag{10}
$$

The oil film temperature is also determined by the direct solution of the linear system presented in Eq. (11), according to the boundary conditions shown in Eq. (12). It is worth mentioning that the mixing temperature condition T_{mix} resulted from the mixing between the replacement fluid and the circulating fluid in the bearing is modeled according to the approach presented by Nicoletti (1999).

$$
\{T\} = [A]^{-1}\cdot\{B\} \tag{11}
$$

$$
\begin{cases}
\left.\dfrac{\partial T}{\partial\eta}\right|_{\eta=1} = 0\\
T\left(0,\eta\right) = T_{mix}\\
T\left(0,\eta\right) = T\left(1,\eta\right)\\
\left.\dfrac{\partial T}{\partial\eta}\right|_{\eta=0} = 0
\end{cases}
\tag{12}
$$

The oil viscosity is calculated along the mesh from the obtained temperature field. The oil viscosity is applied in the Reynolds equation to determine the pressure distribution. Equation (13) presents the relation used to obtain the oil viscosity from the temperature.

$$\mu(T) = a.\exp\left(\frac{b}{T + 273.15 + c}\right) \tag{13}$$

where T is the oil temperature in Celsius degree, a = 1.864 x 10^{-9}, b = 5499, and c = 0.8534 (coefficients a, b, and c calculated for oil ISO VG 68).

As mentioned, the viscosity field is applied on the Reynolds equation and the pressure and temperature fields are recalculated. This process is repeated while the largest difference between the two-step viscosity values is less than a given tolerance. After convergence, the hydrodynamic forces are calculated by integrating the pressure field over the bearing area, as shown in Eq. (14).

$$\begin{Bmatrix} F_x \\ F_y \end{Bmatrix} = -\int_{-L_h/2}^{L_h/2}\int_{0}^{2\pi} p_h \begin{Bmatrix} \cos\theta \\ \sin\theta \end{Bmatrix} R\,d\theta\,dz \tag{14}$$

where z is the axial coordinate and θ is the angular coordinate.

It is important to note that the solution of the pressure field is associated with the balance between the hydrodynamic force and the external loading that is supported by the bearing. In this way, the equilibrium position of the shaft in the bearing, represented by the position E, and the angle of equilibrium α_h (see Fig. 1), are determined when:

$$\vec{F}_W + \vec{F}_h = 0 \tag{15}$$

For a better understanding of the adopted calculation procedure, two flowcharts are shown in Fig. 3. Figure 3a presents the flowchart referring to the HD model, in which the viscosity is considered constant. Figure 3b shows the flowchart referring to the THD model, in which the viscosity is calculated as a function of temperature. In both models, an optimization procedure based on the SQP algorithm (Vanderplaats, 2007) is used to determine the equilibrium position of the shaft (E , α_h).

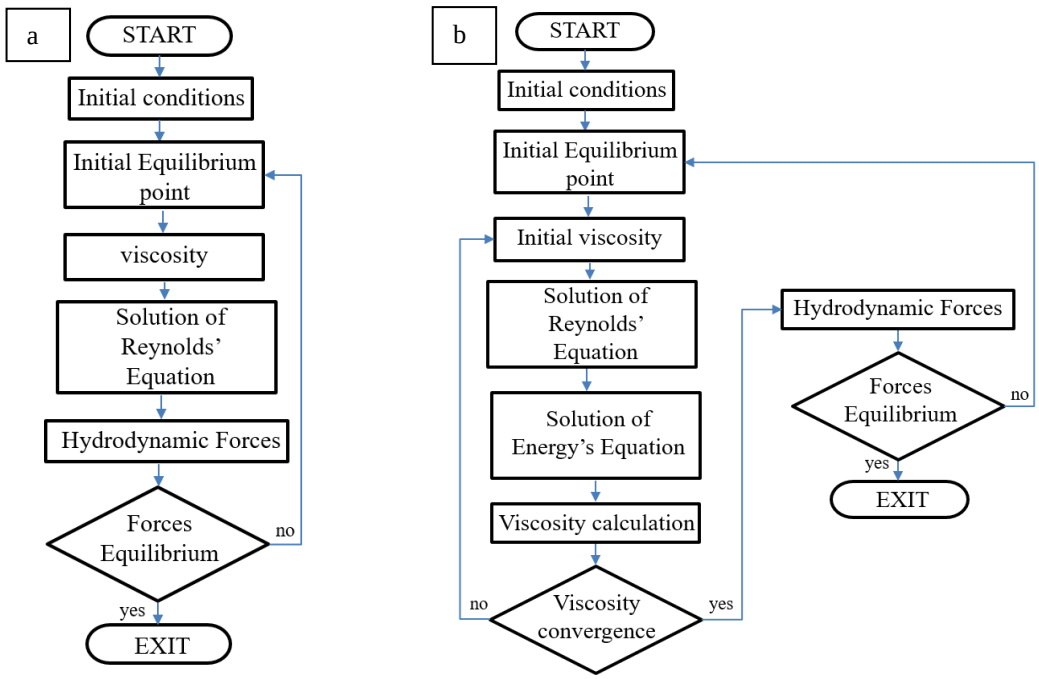

a) HD model. b) THD model.

Figure 3. Flowchart of the force equilibrium convergence process for the HD and THD models.

3. SEQUENTIAL QUADRACTIC PROGRAMMING

According to Vanderplaats (2007), the SQP algorithm is a direct method used for dealing with constrained minimization problems in which the search direction S is found by solving a sub problem with a quadratic objective function and linear constraints. For this aim, a quadratic approximation of the augmented objective function is created (i.e., from the association of the Lagrange multipliers λ with an exterior penalty technique) and a linear approximation for the constraints is written, as shows Eq. (16).

$$\begin{aligned} &\text{Minimize:} \quad Q(S) = F(X) + \nabla F(X)^T S + \frac{1}{2} S^T B S \\ &\text{Subject to:} \quad \nabla g_j(X)^T S + \delta_j g_j(X) \le 0 \qquad j = 1, m \\ &\qquad\qquad\quad \nabla h_k(X)^T S + \bar{\delta} h_k(X) \le 0 \qquad k = 1, l \end{aligned} \tag{16}$$

where X is the vector of design variables and B is initially an identity matrix that will be updated on subsequent iterations. The parameters δ_j and $\bar{\delta}$ are used to prevent inconsistences between the linearized constrains g_j and h_k (i.e., typically $0.9 \le \bar{\delta} \le 0.95$). The δ_j parameter is defined as follows:

$$\begin{aligned} &\delta_j = 1 \quad \text{if } g_j(X) < 0 \\ &\delta_j = \bar{\delta} \quad \text{if } g_j(X) \ge 0 \end{aligned} \tag{17}$$

The direction-finding problem described by Eq. (16) is actually a quadratic programming problem and special techniques should be used for its solution. The associated one-dimensional search is written from the determined search direction S and an exterior penalty function ϕ, as given by Eq. (18).

$$\phi = F(X) + \sum_{j=1}^{m} u_j \{\max[0, g_j(X)]\} + \sum_{k=1}^{l} u_{m+k} \left| h_k(X) \right| \tag{18}$$

where $X = X^{q-1} + \alpha_p S$, $u_j = |\lambda_j|$ ($j = 1, m + l$) in the first iteration, $u_j = \max [|\lambda_j|, 0.5 (u'_j + |\lambda_j|)]$ for the subsequent iterations, and $u'_j = u_j$ from the previous iteration. In this case, $\alpha_p = 1$.

4. NUMERICAL RESULTS

Table 1 shows the geometrical parameters and the operating conditions of the cylindrical bearing used in this work. As mentioned, this bearing is installed in a Francis hydro power unit.

Table 1. Parameters of cylindrical bearing used in the simulations.

Parameters	Value
Bearing diameter [m]	0.5504
Shaft diameter [m]	0.5500
Bearing length [m]	0.440
Radial clearance [m]	2.10^{-4}
Rotation speed [rpm]	300
Radial Load [N]	81,500
Oil type	ISO VG 68
Reference viscosity [Pa.s]	0.0752
Reference temperature [ºC]	40
Inlet oil temperature [ºC]	40
Specific heat capacity of the oil [J/kgºC]	1,890.8
thermal conductivity of the oil [J/s.mºC]	0.1316
Number of volumes along the X direction	50
Number of volumes along the Z direction	50
Number of volumes along the ξ direction	50
Number of volumes along the η direction	10

The number of finite volumes used along the X, Z, ξ, and η directions was obtained from a convergence analysis performed considering the THD model of the bearing. In this case, the number of volumes in the X, Z, and ξ directions were considered equal to define a regular computational mesh. In preliminary tests, the convergence along the η direction was achieved considering 10 finite volumes. In this way, the mesh convergence analysis was devoted to determine the number of volumes in the X, Z, and ξ directions. This analysis was done by means of the errors in the estimation of the bearing forces in the X and Z directions (see Fig. 1), the maximum pressure in the oil film, and maximum temperature. The results of the convergence analysis for the cylindrical bearing are shown in Fig. 4. In this case, the center of the shaft was displaced by 60 μm along the X direction (30% of the radial clearance, see Table 1). Note that the mesh convergence was achieved for $X = Z = \xi = 50$ volumes.

The values of eccentricity, maximum pressure, and minimum oil film thickness calculated according to the HD and THD models were compared and the results are presented in Tab. 2. In this case, the equilibrium position of the shaft was determined considering the radial load presented in Tab. 1. Additionally, regarding the HD model, the oil film temperature was considered constant and equal to the inlet oil temperature (See Tab. 1). As expected, the minimum oil film thickness determined by using the THD model was smaller than the value obtained by using the HD model. The minimum oil film thickness is given by the bearing radial clearance minus the shaft eccentricity. It is also observed that the maximum pressure obtained by using the THD model is smaller than the result determined by the HD model. These differences are associated to the reduction in the viscosity of the oil according to the rise of the temperature.

Figure 5 presents the pressure field obtained by using the HD model. Figure 6 shows the pressure and temperature fields obtained by using the THD model.

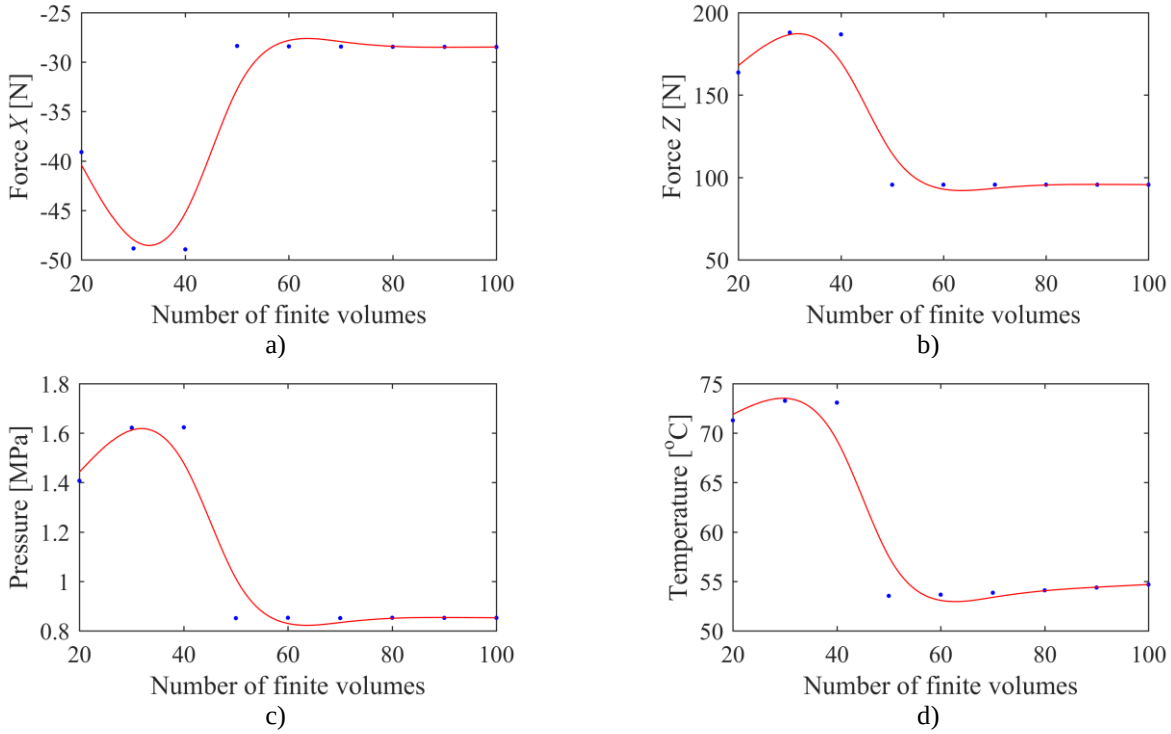

Figure 4. Convergence analysis of the bearing mesh (● obtained results; — fitted curve): a) force in the X direction; b) force in the Z direction; c) maximum pressure; d) maximum temperature.

Table 2. Comparative results between HD and THD models.

Variables	*HD model*	*THD model*	*Difference* [%]
Eccentricity	0.097	0.245	60.41
Angular position [degree]	4.86	5.02	3.19
Maximum pressure [MPa]	0.656	0.653	0.46
Minimum oil film thickness [μm]	180	103	74.76
Maximum Temperature [°C]	-----	52.8	----

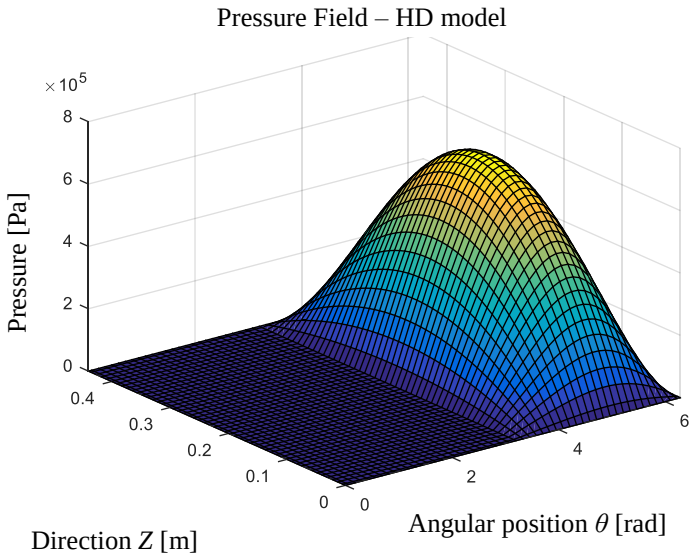

Figure 5. Pressure field obtained by using the HD model.

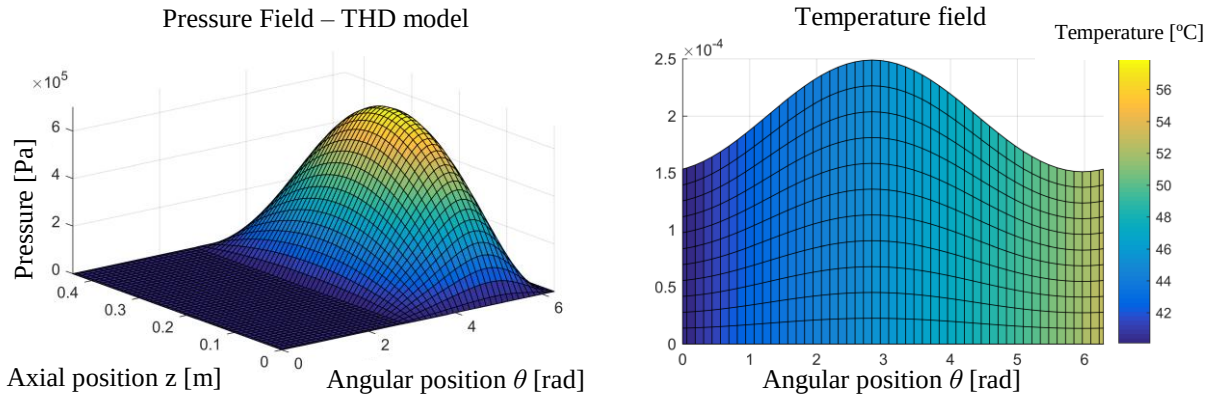

Figure 6. Pressure and temperature fields obtained by using the THD model.

Table 3 presents the results obtained by using the THD model (cylindrical bearing at the equilibrium position) and measured in a Francis hydro power unit (normal operating condition; see Tab. 1). Note that the obtained results are similar to the experimental data, demonstrating the representativeness of the considered THD model.

Table 3. Comparative results between the THD model and the experimental data.

Variables	*THD model*	*Experimental*	*Difference* [%]
Eccentricity	0.245	0.300	18.33
Maximum temperature [°C]	52.8	55.0	4.00

5. CONCLUSIONS

This work was dedicated to the comparation between the results obtained by using the HD and THD models for cylindrical hydrodynamic bearings. In the HD model, the thermal effects in the oil film are disregarded. Differently, in the THD model, the Reynolds equation is solved considering that the oil viscosity can changes due to temperature gradients. The results obtained by using both models were compared in terms of the maximum pressure, minimum oil film thickness, and the equilibrium position of shaft for a given applied load. As expected, different equilibrium positions of the shaft on the bearing were obtained by the considered models. Additionally, the representativeness of the THD model was demonstrated from experimental data measured in a Francis hydro power unit. Further research effort

will be dedicated to the analysis of both bearing models considering the complete rotating machine and, consequently, the associated dynamic effects.

6. ACKNOWLEDGEMENTS

The authors are thankful to the Brazilian Research Agencies FAPEMIG and CNPQ (INCT-EIE) for the financial support provided for this research effort. The authors are also thankful to the companies CERAN, BAESA, ENERCAN, and Foz do Chapecó for the financial support through the R&D project Robust Modeling for the Diagnosis of Defects in Generating Units (02476-3108/2016).

7. REFERENCES

Cavalini Jr, A.A., Lara-Molina, F.A., Sales. T.P., Koroishi, E.H., Steffen Jr, V., 2014. "Uncertainty analysis of flexible rotor supported by fluid film bearings". In *Proceedings of the VIII Congresso Nacional de Engenharia Mecânica – CONEM 2014*. Uberlândia, Brasil.

Childs, D., 1993. *Turbomachinery Rotordynamics: Phenomena, Modeling and Analysis.* John Wiley & Sons, New Jersey.

Daniel, G.B., 2012. *Desenvolvimento de um modelo termohidrodinâmico para análise em mancais segmentados*. Tese de doutorado, Universidade Estudual de Campinas, Campinas.

Maliska, C.R., 2004. *Transferência de Calor e Mecânica dos Fluidos Computacional*. Livros Técnicos e Científicos Editora SA, Rio de Janeiro, 2ª edição.

Meggiolaro, M.A., 1996. *Modelagem de mancais hidrodinâmicos na simulação de sistemas rotativos.* Dissertação de mestrado, Pontifícia Universidade Católica do Rio de Janeiro, Rio de Janeiro.

Riul, J.A., 1988. *Estudo teórico e experimental de mancais hidrodinâmicos cilíndricos.* Dissertação de mestrado, Universidade Federal de Uberlândia, Uberlândia.

Vance, J.M., Zeidan, F.Y. and Murphy, B., 2010. *Machinery Vibration and Rotordynamics*. John Wiley & Sons, New Jersey, 2nd edition.

Vanderplaats, G.N., 2007. *Multidiscipline Design Optimization*. Vanderplaats Research & Development, Colorado Springs.

8. RESPONSIBILITY NOTICE

The authors are the only responsible for the printed material included in this paper.